**Cell Death &
Differentiation**

ARTICLE

Hepatocyte-specific deletion of XBP1 sensitizes mice to liver injury through hyperactivation of IRE1α

Caroline C. Duwaerts[1,2] · Kevin Siao[1,2] · Russell K. Soon Jr[1,2,6] · Chris Her[1,2] · Takao Iwawaki[3] · Kenji Kohno [4] ·
Aras N. Mattis[2,5] · Jacquelyn J. Maher [1,2]

Abstract

X-box binding protein-1 (XBP1) is a transcription factor that plays a central role in controlling cellular responses to endoplasmic reticulum (ER) stress. Under stress conditions, the transcriptionally active form of XBP1 is generated via splicing of *Xbp1* mRNA by the ER-resident protein inositol-requiring enzyme-1 (IRE1α). Genetic deletion of XBP1 has multiple consequences: some resulting from the loss of the transcription factor per se, and others related to compensatory activation of IRE1α. The objective of the current study was to investigate the effects of XBP1 deletion in adult mouse liver and determine to what extent they are direct or indirect. XBP1 was deleted from hepatocytes in adult *Xbp1*^{fl/fl} mice using AAV8-Transthyretin-Cre (*Xbp1*[Δhep]). *Xbp1*[Δhep] mice exhibited no liver disease at baseline, but developed acute biochemical and histologic liver injury in response to a dietary challenge with fructose for 4 weeks. Fructose-mediated liver injury in *Xbp1*[Δhep] mice coincided with heightened IRE1α activity, as demonstrated by *Xbp1* mRNA splicing, JNK activation, and regulated IRE1α-dependent RNA decay (RIDD). Activation of eIF2α was also evident, with associated up-regulation of the pro-apoptotic molecules CHOP, BIM, and PUMA. To determine whether the adverse consequences of liver-specific XBP1 deletion were due to XBP1 loss or heightened IRE1α activity, we repeated a fructose challenge in mice with liver-specific deletion of both XBP1 and IRE1α (*Xbp1*[Δhep];*Ire1a*[Δhep]). *Xbp1*[Δhep];*Ire1a*[Δhep] mice were protected from fructose-mediated liver injury and failed to exhibit any of the signs of ER stress seen in mice lacking XBP1 alone. The protective effect of IRE1α deletion persisted even with long-term exposure to fructose. *Xbp1*[Δhep] mice developed liver fibrosis at 16 weeks, but *Xbp1*[Δhep];*Ire1a*[Δhep] mice did not. Overall, the results indicate that the deleterious effects of hepatocyte-specific XBP1 deletion are due primarily to hyperactivation of IRE1α. They support further exploration of IRE1α as a contributor to acute and chronic liver diseases.

Introduction

X-box binding protein-1 (XBP1) is an important component of the signal transduction network that protects cells against ER stress. XBP1 is positioned downstream of IRE1α (inositol-requiring enzyme-1), one of three canonical ER stress sensors (IRE1α, ATF6, PERK) residing in the ER membrane. IRE1α has kinase and endoribonuclease activities that are unleashed under conditions of ER stress. When IRE1α is activated, its endoribonuclease acts upon *Xbp1* mRNA by splicing a 26-nucleotide fragment that enables translation of a protein termed XBP1s. XBP1s is a transcription factor that induces genes involved in chaperoning proteins through the ER and degrading proteins that cannot

✉ Jacquelyn J. Maher
   Jacquelyn.Maher@ucsf.edu

1   Department of Medicine, University of California San Francisco, San Francisco, CA, USA

2   The Liver Center, University of California San Francisco, San Francisco, CA, USA

3   Division of Cell Medicine, Medical Research Institute, Kanazawa Medical University, Ishikawa 920-0293, Japan

4   Institute for Research Initiatives, Nara Institute of Science and Technology, Ikoma, Nara 630-0192, Japan

5   Department of Pathology, University of California San Francisco, San Francisco, CA, USA

6   Present address: BioMarin Pharmaceutical Inc. 105 Digital Drive, Novato, CA 94949, USA

be properly folded in the ER [1]. XBP1s also induces genes pertinent to phospholipid synthesis, which enhance ER membrane biogenesis and increase the capacity of the organelle [2, 3].

Cell-specific deletion of XBP1 often results in adverse consequences. Deletion of XBP1 from lymphoid precursors prevents the maturation of B cells into plasma cells [4]; deletion from intestinal epithelia predisposes to inflammatory bowel disease [5]; and deletion from CNS neurons promotes leptin resistance and obesity [6]. In these situations, the targeted loss of XBP1 causes enhanced ER stress in the affected cells, which can lead to cell death and associated inflammation. Targeted disruption of XBP1, however, can in some cases lead to mixed positive and negative outcomes. This is true of the liver, in which XBP1 deletion from hepatocytes improves hepatic insulin sensitivity [7] and reduces the hepatic contribution to circulating lipids [8] but sensitizes the liver to pharmacologic ER stress [9] and impairs liver regeneration [10].

One important consequence of XBP1 deletion is hyperactivation of IRE1α [8]. Hyperactivation of IRE1α leads to significant broadening of its endoribonuclease activity, which in turn prompts large-scale degradation of mRNAs in a process called regulated IRE1α-dependent decay (RIDD) [11]. IRE1α hyperactivation also accentuates its kinase activity toward TRAF2, initiating a cascade of events culminating in the activation of JNK and downstream targets such as cJun [12]. Both of these events can trigger cell death. The goal of the current study was to examine the impact of hepatocyte-specific XBP1 deletion in the adult mouse liver, under basal conditions and in response to a mild metabolic stress (fructose feeding). We wished to gain insight into metabolic outcomes as well as cell survival, and to dissect whether the phenotype of XBP1-deficient mice was due primarily to XBP1 loss or to up-regulation of other ER stress pathways.

Methods

Mice and experimental diets

XBP1 conditional knockout mice on a C57BL/6 background ($Xbp1^{fl/fl}$) were obtained from Drs. Ann-Hwee Lee and Laurie Glimcher [8]. IRE1α conditional knockout mice ($Ire1a^{fl/fl}$) were generated as previously described [13] and back-crossed for 10 generations to C57BL/6. The two strains were cross-bred to generate $Xbp1^{fl/fl};Ire1a^{fl/fl}$ conditional knockout mice. At 8 weeks of age, male $Xbp1^{fl/fl}$ or $Xbp1^{fl/fl};Ire1a^{fl/fl}$ mice were injected IV with either 4×10^{11} GC AAV8-Transthyretin-Cre or 4×10^{11} GC AAV8-CMV-null as a control (Vector Biolabs, Malvern, PA).

Gene-deleted mice are designated $Xbp1^{\Delta hep}$ and $Xbp1^{\Delta hep};Ire1a^{\Delta hep}$. Animals were housed for 2 weeks after AAV8 treatment before initiating experimental studies. At 10 weeks of age, mice were placed on either a chow diet (Pico Lab Diets #5053) or a fructose-enriched diet (Envigo TD.89247) for intervals up to 16 weeks. At the end of each experiment, mice were fasted for 4 h before killing. All diet studies contained 4 mice per group; some were repeated for a total of 8 per group. No formal randomization protocol was applied, and investigators were not blinded to the treatment groups. Positive controls for ER stress were generated by injecting adult C57BL/6 mice with tunicamycin (1 mg/kg) and killing them 3 h later. All mouse experiments were performed in accordance with guidelines set by the America Veterinary Medical Association. All mouse studies were reviewed and approved by the Committee on Animal Research at the University of California San Francisco.

Gene expression

RNA was extracted from whole liver in TRIzol (Invitrogen, Carlsbad, CA). RNA was then purified using a Direct-zol RNA Miniprep kit (ZymoResearch, Irvine, CA) and cDNA synthesized as previously described [14]. Gene expression was assessed by quantitative PCR using PrimeTime qPCR assays (Integrated DNA Technologies, Coralville, IA), E@sy Oligo primers (Millipore-Sigma, Burlington, MA) or TaqMan Assays (Life Technology, Carlsbad, CA), followed by normalization to mouse β-glucuronidase. A complete list of primers is cataloged in Table S1. *Xbp1* mRNA splicing was quantitated by measuring spliced and total *Xbp1* mRNA independently in tissue homogenates by QPCR and expressing the ratio as a percentage, as described previously [8, 15].

Histology and immunohistochemistry

Formalin-fixed sections of liver tissue were stained with hematoxylin and eosin. Cell death and proliferation were evaluated by immunohistochemical staining for cleaved caspase-3 and Ki-67. CD68 and myeloperoxidase staining were used to assess the abundance of inflammatory cells in the liver. Stained tissue sections were photographed using a Nikon Microphot microscope (Nikon, Melville, NY) equipped with a SPOT digital camera (Diagnostic Instruments, Inc., Sterling Heights, MI). Caspase-3- and Ki-67-positive cells were counted manually in 10 microscopic fields per liver, and data were reported as the average number of cells per microscopic field. CD68 and myeloperoxidase staining were quantitated as the mean % stained area in 10 microscopic fields per liver (Simple PCI, Hamamatsu Corporation, Sewickly, PA).

Quantitation of hepatic lipids

Lipids were extracted from fresh liver tissue using the Folch method [16]. Total triglyceride was measured spectrophotometrically as previously described (TR0100; Millipore-Sigma) [17].

Quantitation of hepatic fibrosis

Hepatic fibrosis was assessed morphometrically in Sirius Red-stained tissue sections using LAS X (Leica Microsystems, Wetzlar, Germany). The fibrosis area (%) for each liver was assessed as the mean measurement of 6 microscopic fields. Fibrosis was also quantitated by measuring the amount of hydroxyproline in tissue homogenates [18]. Values are reported as mg hydroxyproline/g liver.

Serum tests

Alanine aminotransferase (ALT), total cholesterol, and total triglycerides were measured in mouse serum using an ADVIA 1800 autoanalyzer (Siemens Healthcare Diagnostics, Deerfield, IL) in the clinical chemistry laboratory at the Zuckerberg San Francisco General Hospital.

Western blotting

Livers were homogenized in RIPA buffer containing protease and phosphatase inhibitors. Aliquots were separated by electrophoresis (Bio-Rad TGX, Hercules, CA) and transferred to PVDF membranes (Bio-Rad). Proteins were identified using the following primary antibodies: activating transcription factor 3 (ATF3), activating transcription factor 4 (ATF4), the BH3-only proteins BIM and Bcl-XL, C/EBP homologous protein (CHOP), eukaryotic translation initiating factor 2α (eIF2α), P-eIF2α, cJun, P-cJun, JNK, P-JNK, IRE1α, P- IRE1α, lamin B1, p53 upregulated modulator of apoptosis (PUMA), p38 mitogen-activated protein kinase (p38), P-p38, tubulin, and XBP1. The proteins of interest were visualized by chemiluminescence using a FluorChem FC2 system (Protein Simple, San Jose, CA) and Super Signal West Dura (Thermo Scientific). A complete list of antibodies used for western blotting is included in Table S2.

Statistical analysis

All experimental results were reported as mean ± SEM. Results were compared using analysis of variance (ANOVA) followed by Tukey's multiple comparisons test unless otherwise stated. P values < 0.05 were considered significant. Taking into consideration all measurements in the study, variance was similar among the experimental groups. Statistical analyses were performed with Prism 8.4.3 software (GraphPad Software, San Diego, CA).

Results

AAV8-Transthyretin-Cre successfully deleted XBP1 from hepatocytes in $Xbp1^{fl/fl}$ mice, as shown by the near-complete absence of nuclear XBP1s in the livers of $Xbp1^{\Delta hep}$ mice exposed to inducers of ER stress (Fig. S1A, B). $Xbp1^{\Delta hep}$ mice had low levels of serum lipids (Fig. S1C), which has been reported previously and attributed to impaired hepatic lipid secretion [8, 19, 20]. Liver histology in $Xbp1^{\Delta hep}$ mice was normal (Fig. S1D). When $Xbp1^{\Delta hep}$ mice were fed a fructose-enriched diet for 1 week, lipogenic genes were induced in the liver, although to a lesser extent than $Xbp1^{fl/fl}$ controls (Fig. 1a). Serum cholesterol and hepatic triglyceride levels increased modestly in both groups of mice in response to fructose feeding, but serum triglycerides were unchanged and liver histology and ALT remained normal (Fig. 1b, c).

When fructose feeding was continued for 4 weeks, lipogenic gene expression remained elevated in the livers of $Xbp1^{fl/fl}$ and $Xbp1^{\Delta hep}$ mice with a persistent difference in the magnitude of gene induction between the two groups (Fig. 2a). This was true despite comparable up-regulation of mRNA encoding the transcription factor carbohydrate-response element-binding protein β (ChREBPβ) in $Xbp1^{fl/fl}$ and $Xbp1^{\Delta hep}$ livers upon fructose feeding. Despite their weaker lipogenic gene induction in response to fructose, $Xbp1^{\Delta hep}$ mice displayed evidence of mild hepatic lipid accumulation at the 4-week time point (Fig. 2b, c). Serum lipids in these mice were significantly lower than those measured in fructose-fed $Xbp1^{fl/fl}$ control mice (Fig. 2c). Importantly, fructose-fed $Xbp1^{\Delta hep}$ mice exhibited several features of liver cell death and regeneration. Serum ALT levels rose to three times normal after 4 weeks of fructose feeding; liver histology demonstrated marked lobular disarray with evidence of cell death and regeneration. These were confirmed by immunostaining for cleaved caspase-3 and Ki-67 (Fig. 2b, c). Despite the presence of liver cell death in $Xbp1^{\Delta hep}$ mice, we found little evidence of CD68 immunoreactivity, a marker of macrophage infiltration, at the 4-week time point (Fig. 2b). Liver fibrosis was also absent at this interval (data not shown). The findings in fructose-fed $Xbp1^{\Delta hep}$ mice contrasted with those in fructose-fed $Xbp1^{fl/fl}$ control mice. In control mice, ALT and liver histology remained normal, although their hepatic triglyceride levels did rise above the chow-fed baseline (Fig. 2b, c).

To explore the connection between hepatocyte XBP1 deletion and the development of liver injury in fructose-fed $Xbp1^{\Delta hep}$ mice, we investigated the influence of fructose feeding on the IRE1α-XBP1 axis and the IRE1α target
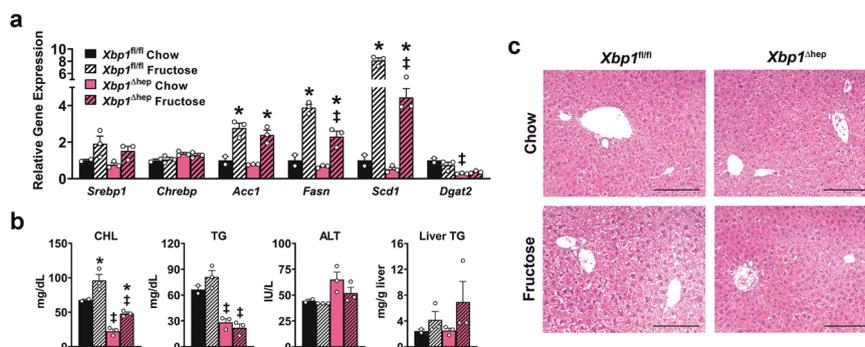
Fig. 1 Response of _Xbp1_^{Δhep} mice to fructose feeding for 1 week. **a** Histogram demonstrates lipogenic gene expression in _Xbp1_^{fl/fl} and _Xbp1_^{Δhep} livers after 1 week of fructose feeding. _Srebp1_ sterol regulatory element-binding protein-1, _Chrebp_ carbohydrate-response element-binding protein, _Acc1_ acetyl-CoA carboxylase-1, _Fasn_ fatty acid synthase, _Scd1_ stearoyl-CoA desaturase-1, _Dgat2_ diacylglycerol O-acyl transferase-2. **b** Graphs depict the corresponding hepatic triglyceride levels after fructose feeding, as well as serum levels of cholesterol (CHL), triglyceride (TG) and ALT. **c** Liver histology following 1 week of fructose feeding. Bar = 200 μm. Values represent mean ± SEM. $P < 0.05$ by ANOVA for _Acc1_, _Fasn_, _Scd1_, CHL and TG. Using Tukey's multiple comparisons test, *$P < 0.05$ for fructose vs. chow of same genotype and ‡$P < 0.05$ for _Xbp1_^{fl/fl} vs. _Xbp1_^{Δhep}.

JNK, which can promote cell death [12, 21]. In _Xbp1_^{fl/fl} control mice, fructose feeding stimulated nuclear translocation of spliced XBP1 (XBP1s) in the liver at 1 week, which disappeared by 4 weeks (Fig. 3a). The early increase in nuclear XBP1s in _Xbp1_^{fl/fl} livers coincided with mild activation of IRE1α, JNK, and cJun but was not associated with significant liver injury (Fig. 2b, c). _Xbp1_^{Δhep} mice, by contrast, contained no detectable XBP1s in the liver at either 1 week or 4 weeks regardless of diet (Fig. 3a). The absence of nuclear XBP1s resulted in significant suppression of several XBP1 target genes as expected [19] (Fig. 3b). Importantly, these same mice displayed robust activation of IRE1α as determined by prominent IRE1α phosphorylation, high levels of _Xbp1_ mRNA splicing and the suppression of RIDD target genes (_Xbp1_ mRNA splicing remains detectable In _Xbp1_^{Δhep} mice because the splice site is not within the sequence deleted by Cre recombinase [8]) (Fig. 3a, c). In _Xbp1_^{Δhep} mice, IRE1α activation was accompanied by the activation of JNK and cJun. P-cJun in particular increased with prolonged fructose feeding and coincided with the development of liver injury (Fig. 3a). This contrasted with p38 MAPK, which was active in all _Xbp1_^{Δhep} livers but also in fructose-fed _Xbp1_^{fl/fl} livers at 4 weeks, independent of IRE1α and JNK activity and liver damage (Fig. 3a).

Because cell death is not exclusively linked to IRE1α and JNK in the setting of ER stress [12, 21], we also investigated the influence of fructose feeding on another death pathway that may be operative in _Xbp1_^{Δhep} mice. We focused specifically on eIF2α, whose activation by eIF2α kinases can lead to cell death by up-regulating apoptotic proteins and downregulating survival proteins. We observed that XBP1 deletion by itself promoted phosphorylation of eIF2α even with chow feeding, as has been reported previously [22]. In chow-fed _Xbp1_^{Δhep} mice, however, eIF2α phosphorylation did not trigger any downstream events such as up-regulation of ATF 3/4 or CHOP (Fig. 4a). The failure of eIF2α to signal induction of AFT3/4 or CHOP has also been reported previously in the livers of _Xbp1_^{Δhep} mice, and attributed to IRE1α-mediated suppression of the eIF2α phosphatase PPP1r15b, via RIDD [22]. When XBP1 deletion was coupled with fructose feeding, eIF2α phosphorylation appeared comparable to that in chow-fed mice. However, in this case, it was accompanied by the induction of ATF3 and ATF4 and up-regulation of the apoptotic proteins CHOP, BIM, and PUMA, without any apparent change in the anti-apoptotic protein Bcl-XL. Together these findings indicate that hepatocyte-specific XBP1 deletion is sufficient to induce activation of IRE1α and eIF2α, but the alterations are without consequence until an exogenous stress such as fructose feeding is applied. This is completely in line with previously published observations [22]. In the presence of fructose, the downstream consequences of XBP1 deletion are associated with hepatic lipid accumulation and liver cell death within 4 weeks. These findings are noteworthy because fructose feeding per se is a mild metabolic challenge, insufficient to provoke a robust or sustained ER stress response in control mice. The experimental results underscore that hepatocyte-specific XBP1 deletion sensitizes the liver to what otherwise would be an innocuous metabolic insult.

Because the activation of IRE1α was so pronounced in the livers of _Xbp1_^{Δhep} mice, we reasoned that it was central to their sensitization to liver injury. To test this directly, we generated mice with AAV8-mediated deletion of XBP1 as well as the RNase domain of IRE1α (_Xbp1_^{Δhep};_Ire1a_^{Δhep}) [13]. _Xbp1_^{Δhep};_Ire1a_^{Δhep} mice expressed a truncated form of IRE1α indicative of the RNase domain deletion [23] (Fig. S2). In contrast to _Xbp1_^{Δhep} mice, _Xbp1_^{Δhep};_Ire1a_^{Δhep} mice exhibited no significant _Xbp1_ mRNA splicing, even

Fig. 2 Response of $Xbp1^{\Delta hep}$ mice to fructose feeding for 4 weeks. a Histogram depicts lipogenic gene expression in the livers of $Xbp1^{fl/fl}$ and $Xbp1^{\Delta hep}$ mice after 4 weeks of fructose feeding. Values represent mean ± SEM. $P < 0.05$ by ANOVA for *Chrebpb*, *Acc1*, *Fasn*, and *Scd1*. Using Tukey's multiple comparisons test, *$P < 0.05$ for fructose vs. chow of same genotype; ‡$P < 0.05$ for $Xbp1^{fl/fl}$ vs. $Xbp1^{\Delta hep}$. **b** Photomicrographs illustrate H&E-stained liver sections as well as immunohistochemistry for cleaved caspase-3, Ki-67 and CD68 in $Xbp1^{fl/fl}$ and $Xbp1^{\Delta hep}$ livers after 4 weeks of fructose feeding. High-power H&E photo illustrates cell death (C) and mitoses (M). Black bar = 200 μm; white bar = 100 μm. **c** Graphs depict quantitative measures of hepatic triglyceride, serum lipids, ALT levels and cell counts for cleaved caspase-3 and Ki-67. Legend as in **a**. Values represent mean ± SEM. $P < 0.05$ by ANOVA for all measurements. Using Tukey's multiple comparisons test, *$P < 0.05$ for fructose vs. chow of same genotype and ‡$P < 0.05$ for $Xbp1^{fl/fl}$ vs. $Xbp1^{\Delta hep}$.
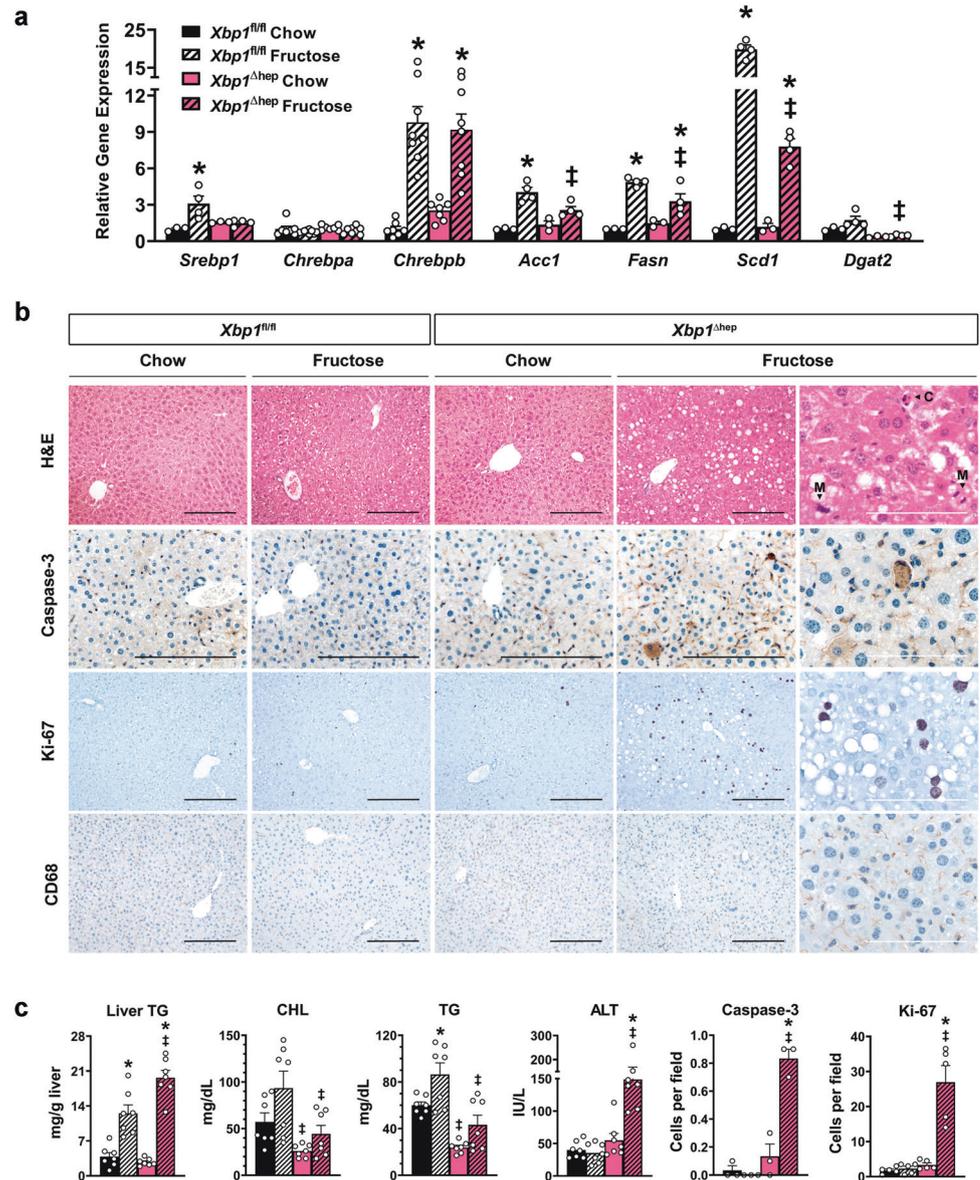
after fructose feeding (Fig. 5a). Several XBP1 target genes were suppressed in the livers of $Xbp1^{\Delta hep}$;$Ire1a^{\Delta hep}$ mice as expected due to the absence of XBP1. RIDD target genes were not suppressed, indicating that RIDD was inactive in the doubly-deficient mice (Fig. 5a). When $Xbp1^{\Delta hep}$;$Ire1a^{\Delta hep}$ mice were challenged with a fructose-enriched diet for 4 weeks, they exhibited a similar profile of lipogenic gene induction as $Xbp1^{\Delta hep}$ mice (Fig. 5b) but did not display the features of ER stress noted previously in $Xbp1^{\Delta hep}$ mice (Fig. 5c). $Xbp1^{\Delta hep}$;$Ire1a^{\Delta hep}$ mice were also spared from fructose-induced hepatic lipid accumulation and liver injury at 4 weeks. Their hepatic triglyceride levels were no higher than those in chow-fed controls, their serum transaminases were normal, and they displayed no evidence of hepatocellular injury by caspase-3 immunostaining (Fig. 6).

This was true despite the presence of hyoplipidemia, indicative of effective gene knockout.

To determine the long-term consequences of XBP1 deletion in hepatocytes, we challenged $Xbp1^{\Delta hep}$ and $Xbp1^{\Delta hep}$;$Ire1a^{\Delta hep}$ mice with fructose vs. chow for 16 weeks. IREα remained active in $Xbp1^{\Delta hep}$ livers and inactive in $Xbp1^{\Delta hep}$;$Ire1a^{\Delta hep}$ livers at 16 weeks (Fig. S3). Single- and double-knockout mice continued to display dampened induction of lipogenic gene expression in response to long-term fructose feeding compared to their respective floxed controls despite similar fructose-mediated induction of *Chrebpb* (Fig. 7a). At 16 weeks, fructose feeding caused modest hepatic steatosis in all mice including the floxed controls (Fig. 7b). Only $Xbp1^{\Delta hep}$ mice, however, developed signs of liver injury, including ALT elevation, macrophage infiltration, and early
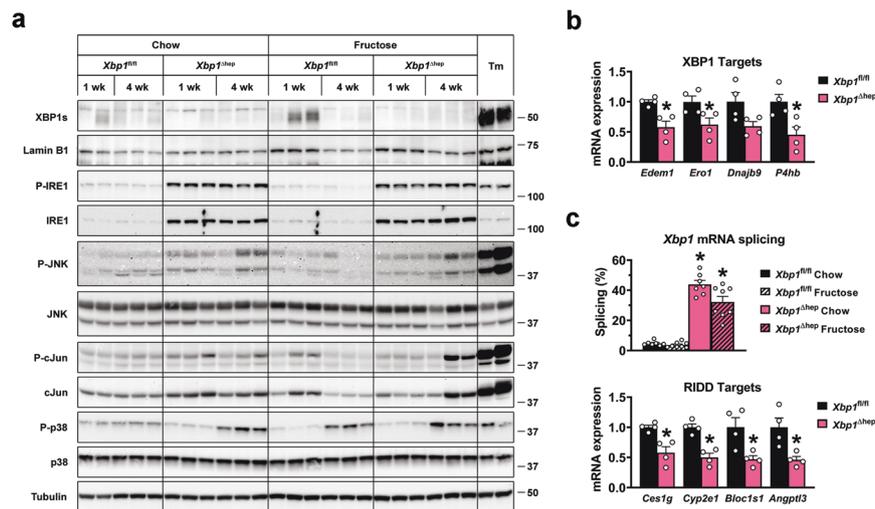
Fig. 3 Effect of XBP1 deletion and fructose feeding on the IRE1α-XBP1 axis. a Western blots illustrate the effects of XBP1 deletion, with or without fructose feeding for 1 or 4 weeks, on activity of the IRE1α-XPB1 axis. Tunicamycin treatment (Tm) served as a positive control. XBP1s and lamin B1 were measured in nuclear extracts; other proteins were measured in whole liver homogenates. In $Xbp1^{fl/fl}$ mice, fructose feeding stimulated nuclear translocation of XBP1s at 1 week but not 4 weeks. This coincided with modest and transient up-regulation of IRE1α and phosphorylation of JNK and cJun. In $Xbp1^{\Delta hep}$ mice, XBP1s was undetectable; IREα was strongly activated regardless of diet or duration. This coincided with activation of JNK and cJun, the latter particularly after 4 weeks of fructose feeding. **b** Graph depicts relative mRNA expression for a panel of direct XBP1

target genes in fructose-fed liver at 4 weeks. *Edem1* ER degradation enhancing alpha-mannosidase like protein 1, *Ero1* ER oxidoreductin 1, *Dnajb9* DnaJ heat shock protein family member B9, *P4hb* protein disulfide isomerase. **c** Graphs depict *Xbp1* mRNA splicing and mRNA expression for a panel of RIDD target genes in the liver at 4 weeks. *Ces1g* carboxylesterase 1g, *Cyp2e1* cytochrome P4502E1, *Bloc1s1* biogenesis of lysosomal organelles complex 1 subunit 1, *Angptl3* angiopoietin-like protein 3. Values represent mean ± SEM. For XBP1 and RIDD targets, *$P < 0.05$ for $Xbp1^{\Delta hep}$ vs. $Xbp1^{fl/fl}$ by unpaired *t*-test. For *Xbp1* mRNA splicing, $P < 0.05$ by ANOVA. Using Tukey's multiple comparisons test, *$P < 0.05$ for chow vs. fructose of the same genotype.
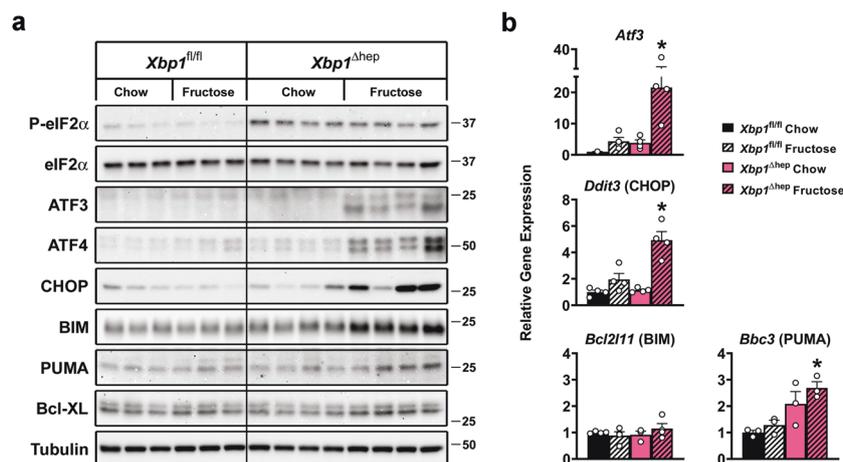

Fig. 4 Effect of XBP1 deletion and fructose feeding on eIF2α and downstream targets. a Western blots illustrate the effects XBP1 deletion, with or without fructose feeding for 4 weeks, on the activity of eIF2α and the expression of several eIF2α targets. $Xbp1^{\Delta hep}$ mice exhibited phosphorylation of eIF2α with chow feeding as well as fructose feeding at 4 weeks. Up-regulation of molecules downstream

of eIF2α occurred only after fructose feeding in $Xbp1^{\Delta hep}$ mice. **b** Graphs demonstrate the transcriptional up-regulation of *Atf3*, *Ddit3*, and *Bbc3* but not *Bcl2l11* in fructose-fed $Xbp1^{\Delta hep}$ mice after 4 weeks. Values represent mean ± SEM. $P < 0.05$ by ANOVA for *Atf3*, *Ddit3*, and *Bbc3*. * $P < 0.05$ for chow vs. fructose of the same genotype.

liver fibrosis (Fig. 7b, c, Fig. S4). Expression of select pro-inflammatory genes was also increased in $Xbp1^{\Delta hep}$ mice (Fig. S4). $Xbp1^{\Delta hep};Ire1a^{\Delta hep}$ mice were protected from the adverse outcomes seen in $Xbp1^{\Delta hep}$ mice (Fig. 7b, c).

Discussion

This study demonstrates that hepatocyte-specific deletion of XBP1 in adult mice renders them susceptible to acute
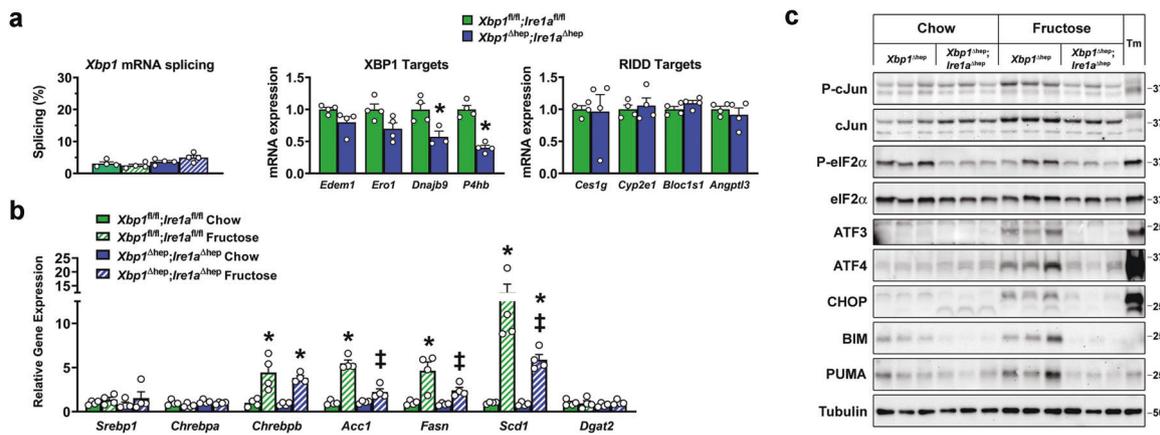
Fig. 5 Characteristics of $Xbp1^{\Delta hep};Ire1\alpha^{\Delta hep}$ mice after 4 weeks of fructose feeding. a Graphs depict $Xbp1$ mRNA splicing and the relative expression of XBP1 and RIDD target genes in $Xbp1^{fl/fl};Ire1\alpha^{fl/fl}$ and $Xbp1^{\Delta hep};Ire1\alpha^{\Delta hep}$ mice after 4 weeks of fructose feeding. Legend for left panel as in **b**. **b** Lipogenic gene expression after 4 weeks of chow or fructose feeding. Values represent mean ± SEM. For lipogenic genes, $P < 0.05$ by ANOVA for $Chrebp$, $Acc1$, $Fasn$, and $Scd1$. Using Tukey's multiple comparisons test, $*P < 0.05$ for chow vs. fructose of the same genotype and $\ddagger P < 0.05$ for $Xbp1^{fl/fl}$ vs. $Xbp1^{\Delta hep}$. For XBP1 and RIDD targets, $*P < 0.05$ for $Xbp1^{fl/fl}$ vs. $Xbp1^{\Delta hep}$ by unpaired t-test. **c** Western blots illustrate the expression of ER stress-related molecules in liver homogenates from $Xbp1^{\Delta hep}$ and $Xbp1^{\Delta hep};Ire1\alpha^{\Delta hep}$ mice after 4 weeks of chow or fructose feeding. Fructose-fed $Xbp1^{\Delta hep}$ mice display phosphorylation of cJun and eIF2α as well as up-regulation of several eIF2α targets. These molecules are not induced in fructose-fed $Xbp1^{\Delta hep};Ire1\alpha^{\Delta hep}$ mice.
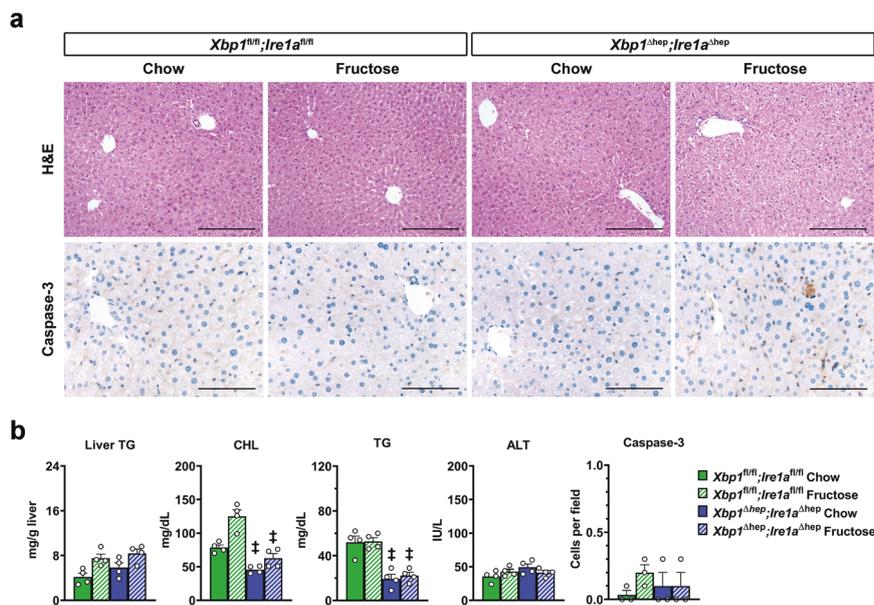

Fig. 6 Fructose feeding does not induce liver injury in mice with dual deletion of XBP1 and IRE1α. a Photomicrographs depict liver histology in $Xbp1^{fl/fl};Ire1\alpha^{fl/fl}$ and $Xbp1^{\Delta hep};Ire1\alpha^{\Delta hep}$ mice after 4 weeks of chow or fructose feeding. There is no evidence of hepatic lipid accumulation and no evidence of liver cell death as assessed by cleaved caspase-3 staining. Bar = 200 μm. **b** Measurements of liver TG, serum ALT, and cleaved caspase-3-positive cell counts confirm the absence of hepatic steatosis or liver injury in $Xbp1^{\Delta hep};Ire1\alpha^{\Delta hep}$ mice. Serum lipids in $Xbp1^{\Delta hep};Ire1\alpha^{\Delta hep}$ mice are suppressed below the values in $Xbp1^{fl/fl};Ire1\alpha^{fl/fl}$ mice. Values represent mean ± SEM. $P < 0.05$ by ANOVA for CHL and TG. Using Tukey's multiple comparisons test, $\ddagger P < 0.05$ for $Xbp1^{fl/fl};Ire1\alpha^{fl/fl}$ vs. $Xbp1^{\Delta hep};Ire1\alpha^{\Delta hep}$.

and chronic liver injury in response to fructose feeding. In $Xbp1^{\Delta hep}$ mice, a mild dietary challenge that was insufficient to cause liver disease in control mice induced significant disease after gene deletion, characterized by hepatic lipid accumulation, liver cell death, and ultimately fibrosis.

Importantly, the susceptibility of $Xbp1^{\Delta hep}$ mice to liver disease was not the direct consequence of XBP1 deletion. Instead, it was due to compensatory up-regulation of the upstream ER stress transducer IRE1α. This was confirmed by liver-specific deletion of both XBP1 and IRE1α, which

a

b

c
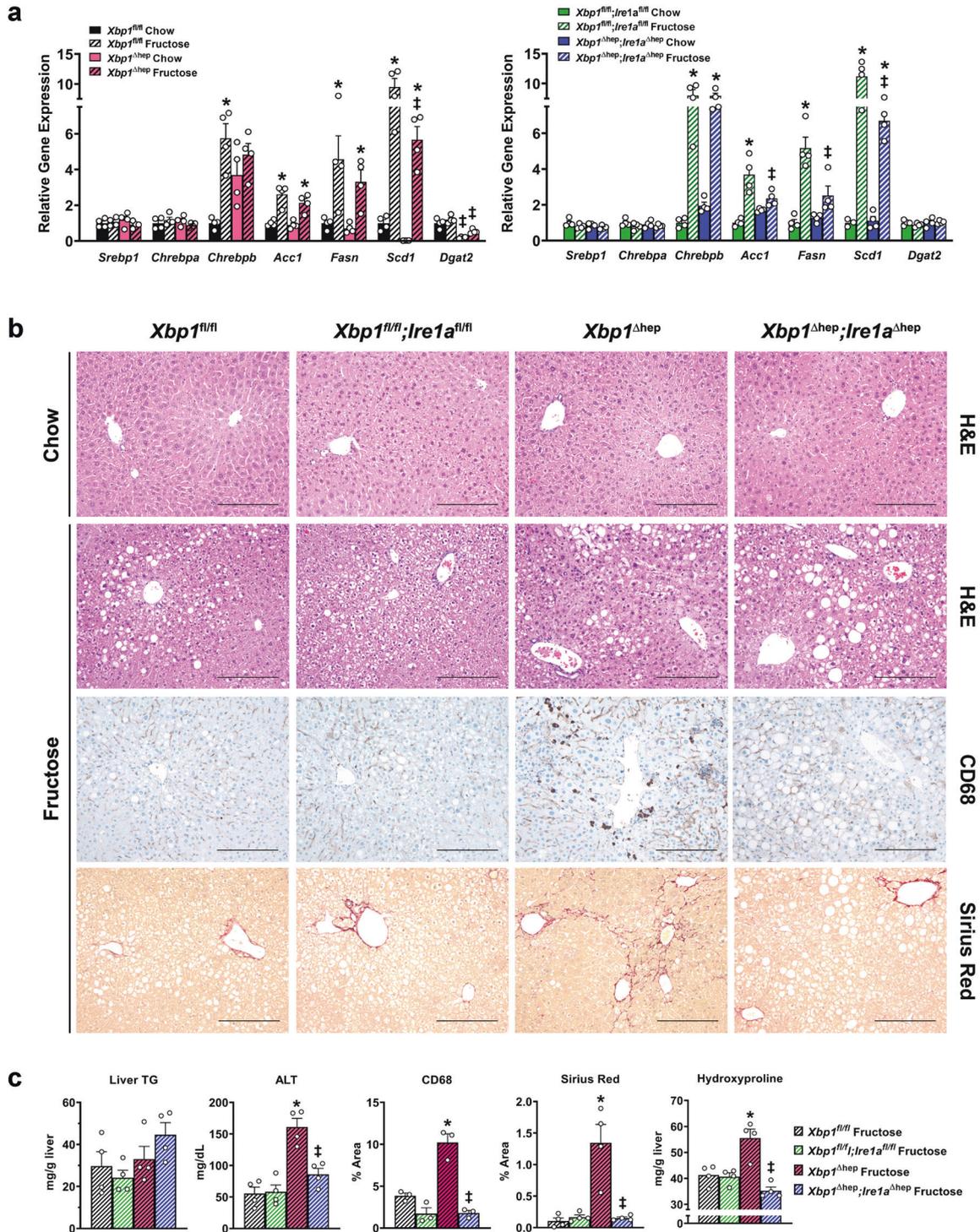
protected mice from the injury observed in mice lacking XBP1.

Fructose-mediated liver injury in $Xbp1^{\Delta hep}$ mice was associated with several features of heightened ER stress, including activation of IRE1α and eIF2α and the induction of the pro-apoptotic molecules JNK and CHOP. All of these stress responses were abrogated by IRE1α deletion, indicating

they were triggered by IRE1α activation. Whether IRE1α provoked liver injury through its kinase or endoribonuclease functions or both is difficult to pinpoint: both were upregulated in our mice, based on the activation of JNK and RIDD. We suspect JNK was activated as a result of IRE1α kinase activity and eIF2α activated as an indirect consequence of IRE1α endonuclease activity (RIDD) [22]. Still, we

◄ **Fig. 7** Long-term consequences of fructose feeding in *Xbp1*$^{\Delta hep}$ and *Xbp1*$^{\Delta hep}$*;Ire1α*$^{\Delta hep}$ **mice. a** Histograms depict lipogenic gene expression in the livers of *Xbp1*$^{fl/fl}$ and *Xbp1*$^{\Delta hep}$ mice or *Xbp1*$^{fl/fl}$*; Ire1α*$^{fl/fl}$ and *Xbp1*$^{\Delta hep}$*;Ire1α*$^{\Delta hep}$ mice after 4 weeks of fructose feeding. Values represent mean ± SEM. $P < 0.05$ by ANOVA for *Chrebpb*, *Acc1*, *Fasn*, and *Scd1;* and for *Dgat2* in single knockout only. Using Tukey's multiple comparisons test, *$P < 0.05$ for chow vs. fructose of the same genotype and ‡$P < 0.05$ for floxed vs. knockout. **b** Photomicrographs demonstrate liver histology in *Xbp1*$^{\Delta hep}$ and *Xbp1*$^{\Delta hep}$*; Ire1α*$^{\Delta hep}$ mice and their floxed controls after 16 weeks of chow or fructose feeding. Chow-fed mice have no obvious histologic abnormalities; fructose feeding induced moderate steatosis in all four groups of mice. CD68 staining shows hepatic inflammation only in fructose-fed *Xbp1*$^{\Delta hep}$ mice. Sirius red staining shows perisinusoidal and bridging fibrosis only in fructose-fed *Xbp1*$^{\Delta hep}$ mice. Bar = 200 μm. **c** Graphs depict liver TG, serum ALT, CD68-stained area and hepatic fibrosis assessed by Sirius Red morphometry and hydroxyproline measurement in control, *Xbp1*$^{\Delta hep}$ and *Xbp1*$^{\Delta hep}$*;Ire1α*$^{\Delta hep}$ mice. The highest values of ALT, CD68 immunoreactivity and fibrosis are in fructose-fed *Xbp1*$^{\Delta hep}$ mice at 16 weeks. Values represent mean ± SEM. $P < 0.05$ by ANOVA for ALT, CD68, Sirius Red morphometry and hydroxyproline. *$P < 0.05$ for floxed vs. knockout; ‡$P < 0.05$ for *Xbp1*$^{\Delta hep}$ vs. *Xbp1*$^{\Delta hep}$*;Ire1a*$^{\Delta hep}$.

acknowledge that these events could occur through other pathways [12, 24, 25]. We also cannot specify which of the several death-promoting molecules induced in *Xbp1*$^{\Delta hep}$ livers were responsible for fructose-induced cell death. JNK, CHOP, BIM, and PUMA were all upregulated on a similar timeline, and thus they all likely contributed collectively to the development of liver injury.

One intriguing observation in the current study was that IRE1α and eIF2α were upregulated at baseline in the livers of *Xbp1*$^{\Delta hep}$ mice, yet there was no evidence of downstream signaling from these two molecules and no liver injury in the absence of an exogenous stimulus. This phenomenon has been reported previously in *Xbp1*$^{\Delta hep}$ mice [22], and supports the notion that some threshold of IRE1α activation must be surpassed, possibly by an exogenous stimulus, in order to effect a cytotoxic response. Some have linked the cytotoxic potential of IRE1α to stress-induced high-order oligomerization of the protein with resultant activation of RIDD [26]. In the current study, however, RIDD was detectable in XBP1-deleted livers even before fructose feeding, and thus RIDD per se cannot be the sole trigger to liver injury. RIDD-induced cell death may be cell-type specific [27, 28], and hepatocytes may be somewhat resistant [19, 29, 30]. Still, our results support the concept that IRE1α activation can be pushed to a level that causes hepatotoxicity, and XBP1 deletion nearly achieves this goal.

It is intriguing that hepatic lipid accumulation occurred in *Xbp1*$^{\Delta hep}$ but not *Xbp1*$^{\Delta hep}$*;Ire1a*$^{\Delta hep}$ mice after short-term fructose feeding, whereas it occurred in both genotypes at 16 weeks. In the single- and double-knockout mice, fructose-induced hepatic lipid accumulation should be influenced in part by diet-induced lipogenesis and in part by

suppression of hepatic lipid secretion, the latter due to down-regulation of the *Xbp1* target gene *P4hb* that plays a role in hepatic VLDL secretion [20]. Our data show no major differences in lipogenic gene induction or *P4hb* suppression between single- and double-knockout mice at 4 weeks (Figs. 2, 3, and 5); however, at this early time point, the amount of lipid measured in the livers of the single-knockout mice was quite small, and thus the mild increase noted in *Xbp1*$^{\Delta hep}$ mice is of unclear significance. Long-term fructose feeding caused more pronounced hepatic lipid accumulation, but in this instance the lipid accrual in *Xbp1*$^{\Delta hep}$ mice was no worse than that in any other group including the floxed controls (Fig. 7c). Still, *Xbp1*$^{\Delta hep}$ mice developed liver injury, inflammation and fibrosis, whereas *Xbp1*$^{\Delta hep}$*;Ire1a*$^{\Delta hep}$ mice were protected. These findings suggest that hepatic lipid accumulation, although a feature of the liver injury seen in fructose-fed *Xbp1*$^{\Delta hep}$ mice, is not itself central to liver damage in this experimental paradigm.

Another interesting observation from our study is that in control mice (*Xbp1*$^{fl/fl}$), fructose feeding induced ER stress only transiently in the liver. In control livers, fructose feeding stimulated the nuclear translocation of XBP1s at 1 week but no longer at 4 weeks; this is in keeping with concept that fructose is a mild stress stimulus, and may explain in part why fructose feeding does not provoke liver injury in control animals. Although ER stress did not persist with prolonged fructose feeding, over time, fructose induced hepatic steatosis in all mice in the study. The uniform steatosis in all mice at 16 weeks underscores that IRE1α activation and associated stress signaling are not absolute prerequisites to fructose-induced hepatic lipid accumulation. Fructose did induce *Chrebpβ* in the livers of all mice in the study, which suggests that fructose-induced hepatic lipogenesis is a strong stimulus to the observed steatosis. Again, these findings support a mechanistic distinction between hepatic steatosis and liver injury our XBP1-deleted mice.

The current work uniquely supplements an existing body of research examining the impact of IRE1α and XBP1 on the liver. Previous studies of liver-targeted deletion of XBP1 have yielded mixed results: some showed no deleterious effect on the liver [8], others showed that XBP1 deletion improved hepatic steatosis in obese mice [19, 31], and still others showed that XBP1 deletion worsened liver injury from pharmacologic or dietary insults [9, 32]. Our experiments are in general agreement with the last group of reports indicating that XBP1 deletion is harmful to the liver when combined with another insult. However, our work diverges from these studies in that we attribute the harmful effect of hepatic XBP1 deletion to IRE1α. When IRE1α is activated to excess, it sensitizes hepatocytes to injurious stimuli.

In summary, the current work underscores the potential for IRE1α to induce liver injury when activated above a threshold level in the proper clinical setting. Indeed, heightened IRE1α activity has been linked to lipotoxic liver injury and nonalcoholic fatty liver disease [33–35]. We believe our experiments have implications extending beyond metabolic liver disease, although they may not be applicable to all forms of liver injury [29]. Nevertheless, our demonstration that IRE1α-mediated liver injury is separable from hepatic steatosis suggests that excess IRE1α activation can contribute to the pathogenesis of other types of ER stress-related liver injury [36–38]. Accordingly, therapeutics targeting excess IRE1α activation may have broad application in the treatment of an array of hepatotoxic diseases.

Compliance with ethical standards

References

1. Lee AH, Iwakoshi NN, Glimcher LH. XBP-1 regulates a subset of endoplasmic reticulum resident chaperone genes in the unfolded protein response. Mol Cell Biol. 2003;23:7448–59.

2. Sriburi R, Jackowski S, Mori K, Brewer JW. XBP1: a link between the unfolded protein response, lipid biosynthesis, and biogenesis of the endoplasmic reticulum. J Cell Biol. 2004;167:35–41.

3. Sriburi R, Bommiasamy H, Buldak GL, Robbins GR, Frank M, Jackowski S, et al. Coordinate regulation of phospholipid biosynthesis and secretory pathway gene expression in XBP-1 (S)-induced endoplasmic reticulum biogenesis. J Biol Chem. 2007;282:7024–34.

4. Reimold AM, Iwakoshi NN, Manis J, Vallabhajosyula P, Szomolanyi-Tsuda E, Gravallese EM, et al. Plasma cell differentiation requires the transcription factor XBP-1. Nature. 2001;412:300–7.

5. Kaser A, Lee AH, Franke A, Glickman JN, Zeissig S, Tilg H, et al. XBP1 links ER stress to intestinal inflammation and confers genetic risk for human inflammatory bowel disease. Cell. 2008;134:743–56.

6. Ozcan L, Ergin AS, Lu A, Chung J, Sarkar S, Nie D, et al. Endoplasmic reticulum stress plays a central role in development of leptin resistance. Cell Metab. 2009;9:35–51.

7. Jurczak MJ, Lee AH, Jornayvaz FR, Lee HY, Birkenfeld AL, Guigni BA, et al. Dissociation of inositol-requiring enzyme (IRE1alpha)-mediated c-Jun N-terminal kinase activation from hepatic insulin resistance in conditional X-box-binding protein-1 (XBP1) knock-out mice. J Biol Chem. 2012;287:2558–67.

8. Lee AH, Scapa EF, Cohen DE, Glimcher LH. Regulation of hepatic lipogenesis by the transcription factor XBP1. Science. 2008;320:1492–6.

9. Olivares S, Henkel AS. Hepatic Xbp1 gene deletion promotes endoplasmic reticulum stress-induced liver injury and apoptosis. J Biol Chem. 2015;290:30142–51.

10. Argemi J, Kress TR, Chang HCY, Ferrero R, Bertolo C, Moreno H, et al. X-box binding protein 1 regulates unfolded protein, acute-phase, and DNA damage responses during regeneration of mouse liver. Gastroenterology. 2017;152:1203–16. e1215.

11. Hollien J, Lin JH, Li H, Stevens N, Walter P, Weissman JS. Regulated Ire1-dependent decay of messenger RNAs in mammalian cells. J Cell Biol. 2009;186:323–31.

12. Tabas I, Ron D. Integrating the mechanisms of apoptosis induced by endoplasmic reticulum stress. Nat Cell Biol. 2011;13:184–90.

13. Iwawaki T, Akai R, Yamanaka S, Kohno K. Function of IRE1 alpha in the placenta is essential for placental development and embryonic viability. Proc Natl Acad Sci USA. 2009;106:16657–62.

14. Pickens MK, Yan JS, Ng RK, Ogata H, Grenert JP, Beysen C, et al. Dietary sucrose is essential to the development of liver injury in the methionine-choline-deficient model of steatohepatitis. J Lipid Res. 2009;50:2072–82.

15. Back SH, Schroder M, Lee K, Zhang K, Kaufman RJ. ER stress signaling by regulated splicing: IRE1/HAC1/XBP1. Methods. 2005;35:395–416.

16. Folch J, Lees M, Sloane, Stanley GH. A simple method for the isolation and purification of total lipides from animal tissues. J Biol Chem. 1957;226:497–509.

17. Lee GS, Yan JS, Ng RK, Kakar S, Maher JJ. Polyunsaturated fat in the methionine-choline-deficient diet influences hepatic inflammation but not hepatocellular injury. J Lipid Res. 2007;48:1885–96.

18. Jamall IS, Finelli VN, Que, Hee SS. A simple method to determine nanogram levels of 4-hydroxyproline in biological tissues. Anal Biochem. 1981;112:70–5.

19. So JS, Hur KY, Tarrio M, Ruda V, Frank-Kamenetsky M, Fitzgerald K, et al. Silencing of lipid metabolism genes through IRE1alpha-mediated mRNA decay lowers plasma lipids in mice. Cell Metab. 2012;16:487–99.

20. Wang S, Chen Z, Lam V, Han J, Hassler J, Finck BN, et al. IRE1alpha-XBP1s induces PDI expression to increase MTP activity for hepatic VLDL assembly and lipid homeostasis. Cell Metab. 2012;16:473–86.

21. Hetz C. The unfolded protein response: controlling cell fate decisions under ER stress and beyond. Nat Rev Mol Cell Biol. 2012;13:89–102.

22. So JS, Cho S, Min SH, Kimball SR, Lee AH. IRE1alpha-dependent decay of CReP/Ppp1r15b mRNA increases eukaryotic initiation factor 2alpha phosphorylation and suppresses protein synthesis. Mol Cell Biol. 2015;35:2761–70.

23. Tsuchiya Y, Saito M, Kadokura H, Miyazaki JI, Tashiro F, Imagawa Y, et al. IRE1-XBP1 pathway regulates oxidative proinsulin folding in pancreatic beta cells. J Cell Biol. 2018;217:1287–301.

24. Taniuchi S, Miyake M, Tsugawa K, Oyadomari M, Oyadomari S. Integrated stress response of vertebrates is regulated by four eIF2alpha kinases. Sci Rep. 2016;6:32886.

25. Timmins JM, Ozcan L, Seimon TA, Li G, Malagelada C, Backs J, et al. Calcium/calmodulin-dependent protein kinase II links ER stress with Fas and mitochondrial apoptosis pathways. J Clin Invest. 2009;119:2925–41.

26. Ghosh R, Wang L, Wang ES, Perera BG, Igbaria A, Morita S, et al. Allosteric inhibition of the IRE1alpha RNase preserves cell viability and function during endoplasmic reticulum stress. Cell. 2014;158:534–48.

27. Lerner AG, Upton JP, Praveen PV, Ghosh R, Nakagawa Y, Igbaria A, et al. IRE1alpha induces thioredoxin-interacting protein to activate the NLRP3 inflammasome and promote

programmed cell death under irremediable ER stress. Cell Metab. 2012;16:250–64.

28. Upton JP, Wang L, Han D, Wang ES, Huskey NE, Lim L, et al. IRE1alpha cleaves select microRNAs during ER stress to derepress translation of proapoptotic Caspase-2. Science. 2012;338:818–22.

29. Hur KY, So JS, Ruda V, Frank-Kamenetsky M, Fitzgerald K, Koteliansky V, et al. IRE1alpha activation protects mice against acetaminophen-induced hepatotoxicity. J Exp Med. 2012;209: 307–18.

30. Maurel M, Chevet E, Tavernier J, Gerlo S. Getting RIDD of RNA: IRE1 in cell fate regulation. Trends Biochem Sci. 2014; 39:245–54.

31. Herrema H, Zhou Y, Zhang D, Lee J, Salazar Hernandez MA, Shulman GI, et al. XBP1s is an anti-lipogenic protein. J Biol Chem. 2016;291:17394–404.

32. Liu X, Henkel AS, LeCuyer BE, Schipma MJ, Anderson KA, Green RM. Hepatocyte X-box binding protein 1 deficiency increases liver injury in mice fed a high-fat/sugar diet. Am J Physiol Gastrointest Liver Physiol. 2015;309:G965–74.

33. Kakazu E, Mauer AS, Yin M, Malhi H. Hepatocytes release ceramide-enriched pro-inflammatory extracellular vesicles in an IRE1alpha-dependent manner. J Lipid Res. 2016;57:233–45.

34. Lebeaupin C, Vallee D, Rousseau D, Patouraux S, Bonnafous S, Adam G, et al. Bax inhibitor-1 protects from nonalcoholic steatohepatitis by limiting inositol-requiring enzyme 1 alpha signaling in mice. Hepatology. 2018;68:515–32.

35. Dasgupta D, Nakao Y, Mauer AS, Thompson JM, Sehrawat TS, Liao CY et al. IRE1A stimulates hepatocyte-derived extracellular vesicles that promote inflammation in mice with steatohepatitis. Gastroenterology. 2020;159:1487–503.

36. Dara L, Ji C, Kaplowitz N. The contribution of endoplasmic reticulum stress to liver diseases. Hepatology. 2011;53:1752–63.

37. Lebeaupin C, Vallee D, Hazari Y, Hetz C, Chevet E, Bailly-Maitre B. Endoplasmic reticulum stress signalling and the pathogenesis of non-alcoholic fatty liver disease. J Hepatol. 2018; 69:927–47.

38. Malhi H, Kaufman RJ. Endoplasmic reticulum stress in liver disease. J Hepatol. 2011;54:795–809.